Ultralow Wear Behavior of Iron–Cobalt–Filled PTFE Composites

Article *in* Tribology Letters · November 2022

DOI: 10.1007/s11249-022-01679-z

CITATIONS
2

READS
144

8 authors, including:

Kylie Elizabeth Van Meter
Florida State University
12 PUBLICATIONS **19** CITATIONS
SEE PROFILE

Tomas F Babuska
Sandia National Laboratories
44 PUBLICATIONS **706** CITATIONS
SEE PROFILE

Christopher Junk
Lehigh University
35 PUBLICATIONS **1,832** CITATIONS
SEE PROFILE

Kasey Campbell
Lehigh University
5 PUBLICATIONS **92** CITATIONS
SEE PROFILE

Tribology Letters (2023) 71:4
https://doi.org/10.1007/s11249-022-01679-z

ORIGINAL PAPER

Ultralow Wear Behavior of Iron–Cobalt-Filled PTFE Composites

Kylie E. Van Meter[1,2] · Tomas F. Babuska[1,2,3] · Christopher P. Junk[4,5] · Kasey L. Campbell[5] · Mark A. Sidebottom[6] · Tomas Grejtak[1,2,3] · Andrew B. Kustas[7] · Brandon A. Krick[1,2]

Received: 20 May 2022 / Accepted: 11 November 2022

Abstract

For the first time, we demonstrate that PTFE filled with iron–cobalt (FeCo) microparticles is an ultralow wear, magnetic, multifunctional tribological material. PTFE filled with 5 wt% of equiatomic, pre-alloyed FeCo powder resulted in steady-state wear rates of 2.8×10^{-7} mm^3/Nm, approaching that of PTFE-filled alumina. Comparable wear rates were not observed for PTFE filled separately with elemental iron (Fe) or cobalt (Co) microparticles. PTFE filled with either Fe or Co microparticles exhibited only incremental improvements in steady-state wear behavior when compared to unfilled PTFE (1 order of magnitude or less improvement). Particle size analysis and morphology indicate that the Fe and Co microparticles are strongly fused agglomerates (5–20 µm) made of smaller primary particles or features, while the FeCo microparticles are large (~40 µm), spherical, dense particles. IR spectroscopy shows that PTFE-FeCo composites form more tribochemical species than elemental Fe- or Co-filled composites, leading to the observed improvements in wear rate. The FeCo particles are surprisingly large as a filler for ultralow wear PTFE. From these results, we conclude that the fully dense, metallic, microscale, and intrinsically brittle FeCo particles may be friable and break down during sliding to reinforce and promote stable tribofilms, akin to the previously reported alumina particles in ultralow wear PTFE-alumina composites.

Keywords PTFE · Friction · Wear · Ultralow wear · Iron · Cobalt · Iron–cobalt · Magnetic

1 Introduction

Polytetrafluoroethylene (PTFE) is a desirable material for tribological applications due to its low friction coefficient ($\mu \sim 0.1$), low surface energy, and large temperature operation ranges [1–5]. During sliding, PTFE adheres to the countersurface, creating a "transfer film" that allows for a low shear-strength interface [6–10]. However, unfilled PTFE exhibits high wear rates on the order of 10^{-4} mm^3/Nm due to large-scale delamination wear of the polymer and instability/poor adhesion of the transfer film to the countersurface. Improvements in wear rate ranging from 100× to 100,000× have been observed when adding filler materials to PTFE, while still maintaining low friction coefficients ($\mu < 0.2$) and many of its desirable material properties [11–25].

The addition of alpha-Al_2O_3 microparticles to PTFE and PTFE-PEEK with concentrations as low as 0.13 wt% has been shown to reduce the wear rates of PTFE–Al_2O_3 composites to $\sim 1 \times 10^{-7}$ mm^3/Nm and PTFE-PEEK–Al_2O_3 composites to $\sim 4 \times 10^{-8}$ mm^3/Nm [22, 26]. Reduction in wear rate with the addition of alumina microparticles has been attributed to the nanoscale aggregate structure of

✉ Brandon A. Krick
bkrick@eng.famu.fsu.edu

1 Mechanical Engineering, Florida Agricultural and Mechanical University - Florida State University College of Engineering, Tallahassee, FL, USA

2 Department of Mechanical Engineering, The Aero-Propulsion, Mechatronics and Energy Center, FAMU-FSU College of Engineering, 2003 Levy Ave, Tallahassee, FL 32310, USA

3 Mechanical Engineering and Mechanics, Lehigh University, Bethlehem, PA, USA

4 CJIdeas, LLC, Wilmington, DE, USA

5 Materials Science and Engineering, Lehigh University, Bethlehem, PA, USA

6 Mechanical and Manufacturing Engineering, Miami University, Oxford, OH, USA

7 Material, Physical, and Chemical Sciences Center, Sandia National Laboratories, Albuquerque, NM, USA

Published online: 25 November 2022

micron-sized particles that can break up due to high-pressure asperity contacts at the sliding interface [15]. Nanoscale filler fragments have been shown to accumulate at the sliding interface [15], creating a mechanically harder, chemically altered, reinforced transfer film and running film [14]. Furthermore, particle size has been shown to be an important variable as microscale fillers impart larger improvements in wear rate than their nano counterparts by arresting subsurface cracks and preventing delamination [15, 27]. Particle size needs to be balanced with particle friability, with studies by Krick et al. showing that highly dense alumina microparticles with high hardness can inhibit the formation of the transfer film by abrading the countersurface [15, 28].

Understanding the effects of filler particle size and mechanical properties on PTFE–alumina composites can give insight into desirable properties of fillers to create other ultralow wear PTFE composites. As sliding-induced shear drives filler particle fragmentation and chain scission of PTFE polymer chains, tribochemistry at the sliding interface driven by bonding of carboxylic end groups to the metallic oxides of the filler material results in ultralow wear rate PTFE–alumina composites [14]. However, the ultralow wear rates observed in metal-filled PTFE composites suggest that the presence of metal oxide fillers is not required for ultralow wear. In recent studies by Ullah et al., PTFE filled with titanium, chromium, and manganese microparticles slid against brass exhibited ultralow wear rates (2×10^{-9}–2×10^{-7} mm^3/Nm) [29]. Bronze is the most commonly used metallic filler in PTFE composites for industrial applications. High weight percent (40–60%) bronze fillers in PTFE are used in linear bearing applications and exhibit wear rates of ~ 3×10^{-7}mm^3/Nm [10, 30–37]. PTFE–bronze has excellent thermal conductivity but low electrical conductivity and has no intrinsic magnetic properties. Currently, there are no ultralow wear PTFE composites made with magnetic or electrically conductive filler materials.

Iron–cobalt (FeCo) alloys are electrically conductive and, depending on the ratio of Fe to Co, have the highest mean atomic moment, and thus magnetization saturation, of any commercially available soft magnetic alloy. For example, Fe–50Co (referred to hereafter as FeCo) has a high saturation induction B_{max} = ~ 2.4 T) while retaining high permeability (~ 8×10^3) and low coercivity (~ 100 A/m), magnetic properties that are well suited for a range of electromagnetic applications, such as motors, transformers, and solenoids [38–40]. However, FeCo alloys, especially at the near-equiatomic composition, are brittle (< 5% strain to fracture in tension) due to a disorder–order phase transformation, making them difficult to process in bulk form, and use in mechanically demanding applications unless alloyed with other elements, like vanadium, chromium, or niobium, among others [41]. The alloying of other elements with FeCo improves the mechanical properties but decreases some of the desirable magnetic properties. For instance, FeCo alloys with a modest 3% niobium addition can exhibit > 10% lower saturation magnetization and > 600% higher coercivity compared to binary FeCo [39]. For tribological fillers, however, brittle materials can be advantageous in the development of transfer films through the breakdown and accumulation of the filler material at the sliding interface. The combination of brittle material properties with the magnetic and electrical properties of FeCo presents an interesting multi-faceted tribological filler material for PTFE composites. In this manuscript, $Fe_{0.5}Co_{0.5}$ microparticles are used to create a PTFE–FeCo composite. The powders' particle size and morphology were analyzed to understand the structure of the powders. Friction and wear testing were performed to compare the tribological behavior of PTFE–Fe, PTFE–Co, and PTFE–FeCo. IR spectroscopy of both the worn and unworn surfaces of the composites was used to observe potential tribochemical changes in the tribofilms formed through sliding.

2 Materials and Sample Preparation

Three polymer composite samples were prepared, PTFE (Chemours Teflon® 7C resin) filled with 5 wt% FeCo, 5 wt% Fe, and 5 wt% Co. A custom FeCo powder from Sandvik Osprey Powders consisting of alloyed equiatomic $Fe_{0.5}Co_{0.5}$ (particle size 45 ± 15 μm) was used, as well as Fe powder (Sigma-Aldrich Iron 97%, 325 mesh ~ 44 μm particle size) and Co powder (Merck Cobalt Powder 99+, 1–5 μm particle size). To create the composite powder mixture, the dry powder components were combined, and isopropyl alcohol (IPA) was added in a 5:1 (IPA to powder) ratio by mass. The solution was initially mixed with a spatula to create a slurry. To fully disperse the powder in the slurry, the samples were sonicated using an ultrasonic horn equipped with a micro-tip (Branson Digital Sonifier SFX550) for three continuously pulsed 5-min cycles at 40% amplitude with a 1-min rest between cycles. The sonicated composite powder samples were placed in a fume hood for approximately 3–5 days to allow all IPA to evaporate from the sample.

After drying, 10 g of composite powder was placed in a 12.7-mm-diameter 440C stainless steel cylindrical mold and compressed to 30 MPa using a hydraulic press at room temperature. An unfilled PTFE cylinder was also molded using the same method. The molded cylinder was then wrapped in aluminum foil and free sintered in an oven, ramping from room temperature to 380 °C at 2 °C/min, with a dwell at 380 °C for 3 h, and cooled at 2 °C/min to room temperature. The free sintered cylinder was machined into a 12.7 × 6.35 × 6.35 mm polymer pin. Prior to testing, each pin was sonicated in methanol for 30 min and allowed to air dry.

The counter sample used in testing consisted of a 304 stainless steel coupon (4.8 mm × 25.4 mm × 38.1 mm) that

was polished to a mirror finish. Using a scanning white light optical profilometer, the surface roughness was determined to be 25 nm R_a. Each counter sample was washed using Alconox soap and water and rinsed with methanol to remove any surface contamination, and then allowed to air dry.

3 Methods

3.1 Friction and Wear

Wear and friction experiments were performed on a bi-directional linearly reciprocating tribometer in a flat-on-flat sample configuration (Fig. 1). A normal load of 250 N (6.2 MPa) was applied to the polymer composite pin using a ball-screw-driven stage connected to a laterally constrained cantilevered flexure. Applied load and resultant friction force were measured using two decoupled load cells and active servo-on-load was utilized to maintain constant loading conditions. A ball-screw stage was used to slide the counter sample below the polymer composite pin at a speed of 50 mm/s and a stroke length of 25 mm (50 mm/cycle). Samples underwent sliding for the following cycle intervals: 1 k, 4 k, 5 k, 10 k, 10 k, 10 k, 10 k, 50 k, 100 k, 100 k, 100 k, 100 k, for a total of 500 k cycles (total distance 25 km). Due to extremely high wear rates, some samples were only able to be tested up to 50 k total sliding cycles. Sliding experiments were performed in a controlled environment with a relative humidity of $30 \pm 1\%$.

Before testing, each sample was measured with calipers (Mitutoyo AOS, 0.01 mm resolution) and weighed on a scale (Mettler Toledo XS205DU, 0.00001 g resolution) to determine material density. After each cycle interval, samples were removed from the tribometer and weighed on the scale. Calculated density (using initial sample dimensions and weight), and subsequent mass loss were used to calculate volume loss of the sample. The specific wear rate of the sample (K) was calculated using Eq. 1, where V is the volume loss of sample, F_N is the applied load, and d is the sliding distance.

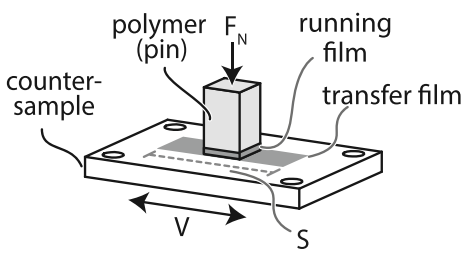

Fig. 1 Flat-on-flat sample configuration, demonstrating a polymer pin sliding against a stainless steel counter sample with an applied normal load F_N, stroke length S, and reciprocating velocity V

$$K\left[\mathrm{mm}^3/\mathrm{Nm}\right] = \frac{V\left[\mathrm{mm}^3\right]}{F_N[\mathrm{N}]d[\mathrm{m}]} \quad (1)$$

Total wear rate (K_{tot}) was calculated using the total lost volume of the sample and the total sliding distance for the entire experiment lifetime. Incremental wear rates (K_{inc}) were calculated using the volume loss per test segment and the distance traveled for that test segment. Steady-state wear rates (K_{ss}) and associated uncertainties were calculated through Monte Carlo simulations [42, 43]. All steady-state wear rates reported were calculated in the regions of linearly increasing volume loss, fitting the Monte Carlo simulations to the final four points of volume loss for each sample. Total wear rate demonstrates the overall performance of the sample while incremental wear rate shows performance of the sample as a function of incremental sliding cycles. Steady-state wear rate is determined when the sample reaches linear volume loss behavior.

Friction coefficients and their standard deviations were calculated using methods described in [44]. Friction loops were generated by dividing the measured friction force by the applied normal force throughout each sliding cycle and were used in the calculations for reported friction coefficient.

3.2 Infrared Spectroscopy

A PerkinElmer Spectrum 100 Fourier Transform Infrared (FT-IR) Spectrometer with an Attenuated Total Reflectance (ATR) accessory was used to identify the chemical changes that occurred on the polymer wear surface (running film, Fig. 1) of tribologically tested PTFE–Fe, PTFE–Co, and PTFE–FeCo composites. Prior to spectra collection, the ATR diamond crystal was cleaned with isopropyl alcohol followed by a background scan to subtract unwanted residual peaks from the sample spectrum. During ATR measurements, the polymer sample surface was placed in contact with the diamond crystal and a normal force was applied using a manual probe. Spectra collected consisted of 32 scans with a spectral resolution of 4 cm^{-1}. Baseline subtraction was performed using the PerkinElmer Spectrum software's baseline subtraction feature.

A Harrick SplitPea™ ATR microscope interfaced with a PerkinElmer Spectrum One Fourier transform infrared spectrometer utilized in reflectance mode was used to identify the chemical composition of polymeric transfer films (Fig. 1) formed on the stainless steel counter sample after sliding. 16 scans with a spectra resolution of 4 cm^{-1} were collected. The PerkinElmer Spectrum software's baseline subtraction feature was used to perform a baseline correction.

3.3 Particle Size Analysis and Morphology

A Malvern MasterSizer LASER (Light Amplification by Stimulated Emission of Radiation) diffractor was used to perform particle size analysis on the Fe, Co, and FeCo powders. A volume distribution was calculated from the LASER diffraction pattern of a suspension of particles. Prior to measurement, ~ 350 mg of each powder was added to 20 mL of a non-aqueous carrier solution with a surfactant. Samples were pipette mixed to evenly disperse the particles. Due to the magnetic nature of the particles, analysis was performed at the highest recirculation speed to prevent particles from clustering together.

A FEI Helios G4 UC Field Emission Scanning Electron Microscope (FESEM) was used to image the Fe, Co, and FeCo filler particles. Powders were deposited on double-sided carbon tape. Secondary electron images were acquired at 3 keV using the Everhart–Thornley detector (ETD) with a 5 µs dwell time.

3.4 Profilometry

Profilometry measurements of the stainless steel substrates were performed using a Bruker Contour GT optical profilometer. A 10 mm × 2.32 mm region of the transfer film was scanned using the 5× objective and white light source, with a pixel size of 3.6 µm. Line scans obtained were averaged over the length of the transfer film to determine an average film profile.

4 Results

4.1 Filler Particle Size and Morphology

The iron (Fe), cobalt (Co), and iron–cobalt (FeCo) powders were imaged using a scanning electron microscope (SEM) with a secondary electron detector to visualize particle size and morphology (Fig. 2a–c). The Fe powder appears to have large particles of about 10–40 µm in size (Fig. 2b). Upon closer inspection, the particles appear to have a smaller, irregularly shaped feature size of approximately 1–2 µm; it is possible that this is a strongly fused agglomerate of smaller particles. The Co powder has smaller bulk particles in the 5–15 µm range (Fig. 2a), which also appear to have a smaller feature size that are more spherical in shape and smaller than the Fe particle features, ranging from 1 µm down to larger nanoscale particles (order 700 nm). In contrast, the FeCo powder particles are large, in the 20–50 µm range, and are uniform and spherical (Fig. 2c). There appear to be very few small (5–10 µm) features on the surface of the large particles, and the overall bulk particle shape is uniform.

Laser diffraction results support the particle size and morphology observed in the SEM images (Fig. 2d, e). Volume-based (Fig. 2f: *i–iii*) and number-based (Fig. 2f: *iv–vi*) diameter differential distribution (i.e., probability distribution; Fig. 2d) and cumulative distribution (i.e., cumulative probability; Fig. 2e) were computed. Both the differential and cumulative distributions show that based on volume, the mean, median, and mode particle size are measured to be larger than the same values calculated based on particle number (Fig. 2d, e). The shift in the Co and Fe distribution curves demonstrates that while by volume the median particle size is ~ 8 and 20 µm (respectively), there are a high number of small diameter, low volume particles present. This causes the Co and Fe median particle diameter to shift to 1.2 and 2.4 µm (respectively). These number-weighted values coincide with the primary feature size observed in SEM. The FeCo powder number-based distribution is also shifted slightly to smaller particle diameters, but the distribution shape is remarkably similar to the volume-based distribution, most likely due to the more uniform particle shape and size observed in SEM and the lack of many small particles/features.

The differential volume density distribution of the Fe powder spans across a wide range of particle sizes (1–80 µm) (Fig. 2d, f). The mean volume-weighted particle size was calculated to be 24.5 µm. Only 10% of the volume of particles are smaller than 7.80 µm, and less than 0.5% of the powder volume has particles smaller than 2 µm (Fig. 2e: *ii*). However, by number, ~ 50% of the particles fall below 2 µm (Fig. 2f: *v*), a diameter which is similar to the primary feature size seen in SEM (Fig. 2b). This could indicate that there are a large number of particles that fall into the category of the primary feature size, and that the larger particles could be hard agglomerates of smaller particles. The manufacturer reports a mesh size of 325 (44 µm), and 93% of the particles by volume have diameters which are equal to or less than the value given by the manufacturer. While the manufacturer reports an accurate mesh value that matches the measured cumulative distribution by volume (Fig. 2e: *ii*), it should be noted that based on a number-weighted distribution, 90% of the particles are less than 7.57 µm, much smaller than the reported value (Fig. 2e: *v*).

The Co powder also has a differential volume density distribution that spans a broad range of particle sizes, from 0.6 to 35 µm (Fig. 2d). However, the volume density percentiles are more closely grouped, with a mean volume-weighted particle size of 9.79 µm and 90% of the powder volume contains particles under 15.9 µm in diameter (Fig. 2e, f). Only 10% volume percent of particles fall below 4 µm in diameter. The manufacturer reports particle sizes in the range of 1–5 µm, but the differential volume

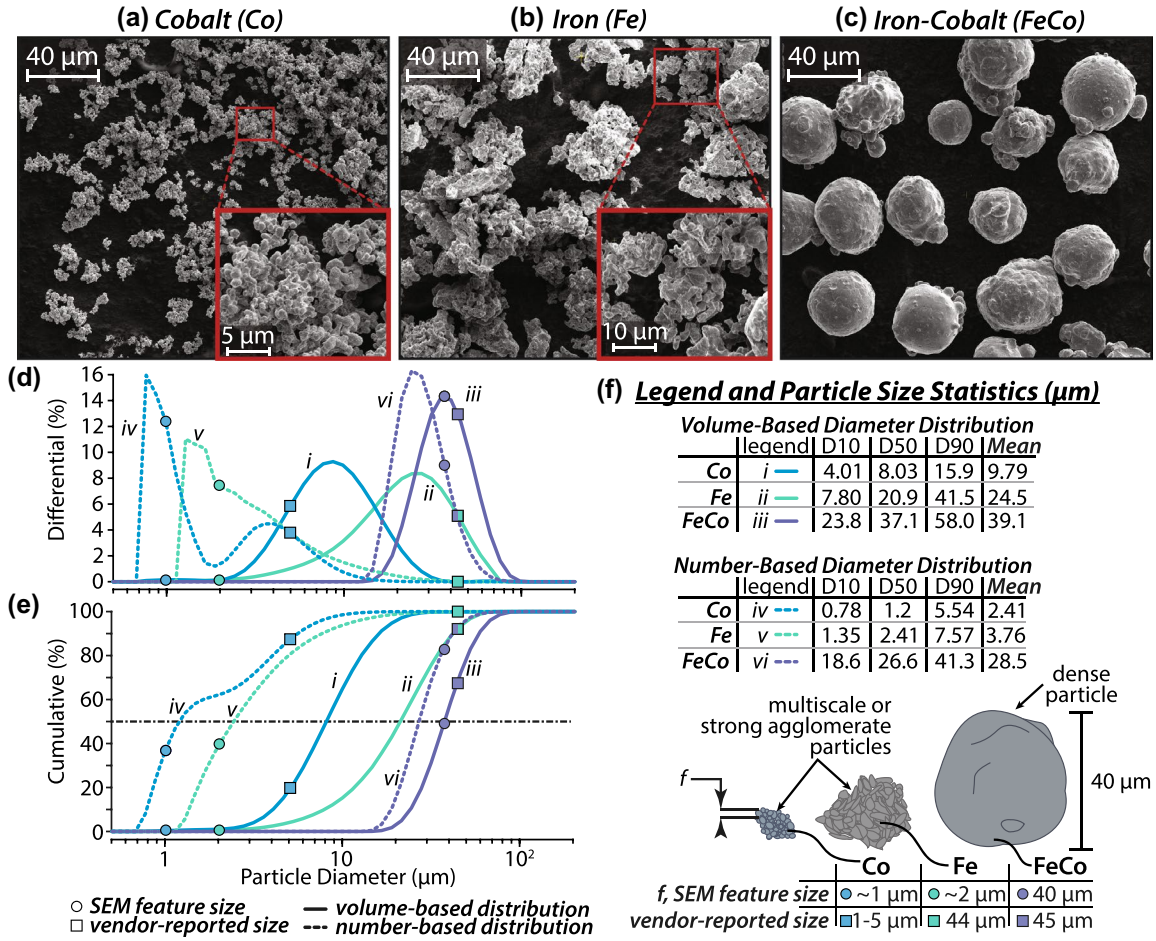

Fig. 2 SEM secondary electron images of the three filler powders: **a** cobalt (Co), **b** iron (Fe), and **c** iron–cobalt (FeCo). Particle diameter distributions measured by laser diffraction and computed as volume and number weighted **d** differential distributions and **e** cumulative distributions. Observed SEM primary feature size and vendor-reported particle size are indicated on the distribution curves. **f** Legend and particle size statistics, including 10th, 50th, and 90th percentiles and mean for (*i–iii*) volume-based diameter distributions and (*iv–vi*) number-based diameter distributions. Relative size and morphology of Co, Fe, and FeCo particles are illustrated

density distribution as well as SEM images indicate that the volume-weighted average particle size is larger than the value given by the manufacturer; as such, we hypothesize that the manufacturers use an adsorption method to approximate particle size by measuring the surface area and mass of the particles and approximating them as spherical [15]. The Co powder has a second differential peak at around 1 µm that is less visible in the volume-weighted distribution but becomes the primary peak in the number-weighted distribution (Fig. 2f: *i*, *iv*). This peak indicates that ~ 1% of a given volume of powder contains particles less than 2 µm in size, but that ~ 60% of a given number of particles fall into this category. These small particle sizes match the primary features that make up the larger strongly fused agglomerate particles which can be seen using SEM (Fig. 2a). The separation of the peaks at 1 µm and 5 µm could indicate that the cobalt powder is made up of mostly strongly fused larger agglomerates and smaller primary particles, with few particles that fall in between (Fig. 2d: *iv*).

The FeCo differential volume density distribution includes particles from 12 to 100 µm (Fig. 2d: *iii*). The powder has a mean volume-weighted particle size of 39 µm with 90% of the a given powder volume having a particle less than 58 µm (Fig. 2e, f: *iii*). Unlike the Fe and Co powders, the smallest particle sizes of the FeCo particles are on the order of 10 µm, with only 10% of the particles by volume falling below 23.8 µm in size. By number, 90% of particles are less than 41 µm in size, and the mean particle size is 28.5 µm (Fig. 2e, f: *vi*). This result, along with SEM imaging of the particles, show that the FeCo powder is comprised of micron scale particles that are not agglomerates, but rather dense uniform spherical particles. An illustration of the observed particle morphology and volume-weighted mean particle size is shown in Fig. 2f, where the Fe and Co agglomerate particles are on average 24.5 and 9.79 µm,

respectively, and are comprised of micron scale primary features, while the FeCo particles are on average 39 µm in diameter and are uniform, dense spheres. The FeCo particle manufacturer reported size is 45 µm (± 15 µm), which appears to be larger than the particles observed in the SEM and the median and mean particle diameter measured with laser diffraction. However, the reported size and range does fall within the volume-weighted cumulative distribution.

4.2 Wear and Friction Behavior

The steady-state wear rate of the PTFE 5 wt% Fe sample was found to be 1.8×10^{-4} mm^3/Nm with an average friction coefficient of 0.17 (Fig. 3a, b). PTFE 5 wt% Co achieved a steady-state wear rate of 7.4×10^{-5} mm^3/Nm, ~2× lower than the wear rate of 5 wt% Fe, but had a slightly higher average friction coefficient ($\mu_{ss} = 0.19$). The composite filled with 5 wt% FeCo achieved a steady-state wear rate of 2.8×10^{-7} mm^3/Nm and an average friction coefficient of 0.21, the lowest wear rate of all composites tested, and a 100×–1000× reduction in wear compared to the Co and Fe composites, respectively. The wear rates for all three PTFE composites are shown in Fig. 3a and tabulated in Table 1. An inverse relationship between friction coefficient and wear rate was observed for all samples tested. All composite samples exhibited lower wear rates when compared to the unfilled PTFE control.

Steady-state wear was calculated using a four-point fit through the linear region of volume loss for each sample. Steady-state friction coefficient μ_{ss} is the average friction coefficient during the steady-state wear region.

Wear testing of the PTFE–Fe and PTFE–Co samples was concluded after 50 k sliding cycles (2.5 km distance) due to high wear rates causing excessive volume loss. As shown in Fig. 4a, the volume loss of the PTFE–Fe sample is linear on a log–log plot of the sliding distance vs. volume loss. There was no observable run-in behavior for the PTFE–Fe sample which achieved steady-state wear in the early stages of testing. The constant wear rate behavior is observed in Fig. 4b and is shown by an unchanged incremental wear rate of the PTFE–Fe sample over its entire sliding distance except for minor fluctuations. The PTFE–Co sample showed minor run-in in the first 1 km of sliding, after which the incremental wear rate of the sample became constant (Fig. 4b) and a steady-state wear rate (7.4×10^{-5} mm^3/Nm), ~2× lower than the PTFE–Fe sample and 10× lower than the unfilled PTFE sample was achieved.

Testing of the PTFE–FeCo sample was carried out for 500 k sliding cycles (50 km), 10× longer than the PTFE–Fe and PTFE–Co samples. After the first 1 k sliding cycles, the PTFE–FeCo sample experienced a high amount of volume loss (~4 mm^3) (Fig. 4a), more than PTFE–Fe (~3 mm^3) or PTFE–Co (~3.2 mm^3). After 1 k sliding cycles, the incremental volume loss for PTFE–FeCo decreased and the incremental wear rate of the PTFE–FeCo sample dropped ~100× over the following 250–500 m of sliding

Table 1 Steady-state wear K_{ss}, steady-state friction μ_{ss}, for unfilled PTFE and Fe, Co, and FeCo PTFE composites

Material	K_{ss} (mm^3/Nm)	μ_{ss}
5 wt% Fe	$1.8 \pm 0.01 \times 10^{-4}$	0.17 ± 0.01
5 wt% Co	$7.4 \pm 0.09 \times 10^{-5}$	0.19 ± 0.01
5 wt% FeCo	$2.8 \pm 0.10 \times 10^{-7}$	0.21 ± 0.01
Unfilled PTFE	$7.8 \pm 0.01 \times 10^{-4}$	0.18 ± 0.01

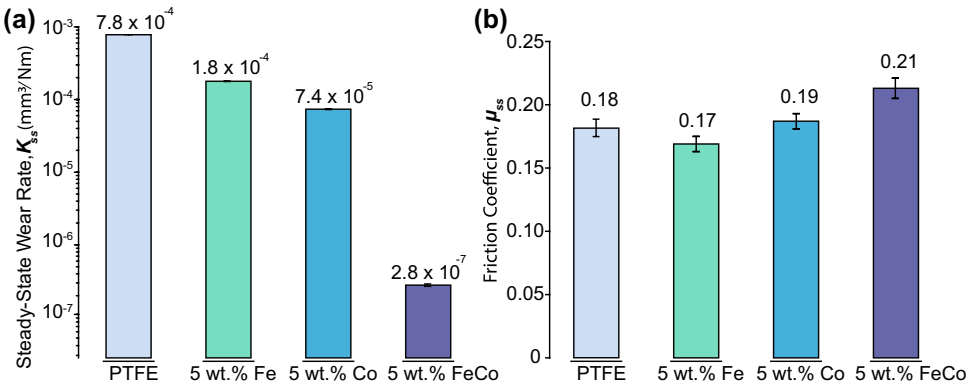

Fig. 3 **a** Steady-state wear rates for unfilled PTFE, and PTFE filled with 5 wt% Fe, 5 wt% Co, and 5 wt% FeCo. Steady-state wear was calculated using a four-point Monte-Carlo simulation fit during the linear region of volume loss for each sample. Error bars represent the uncertainty of the calculation. It should be noted that the error bars are not very visible because wear rate uncertainty for each sample is one or more orders of magnitude smaller than the measurement itself. **b** Average friction coefficient in the steady-state wear region for unfilled PTFE, and PTFE filled with 5 wt% Fe, 5 wt% Co, and 5 wt% FeCo. Error bars indicate the standard deviation of the friction coefficient over the averaged region

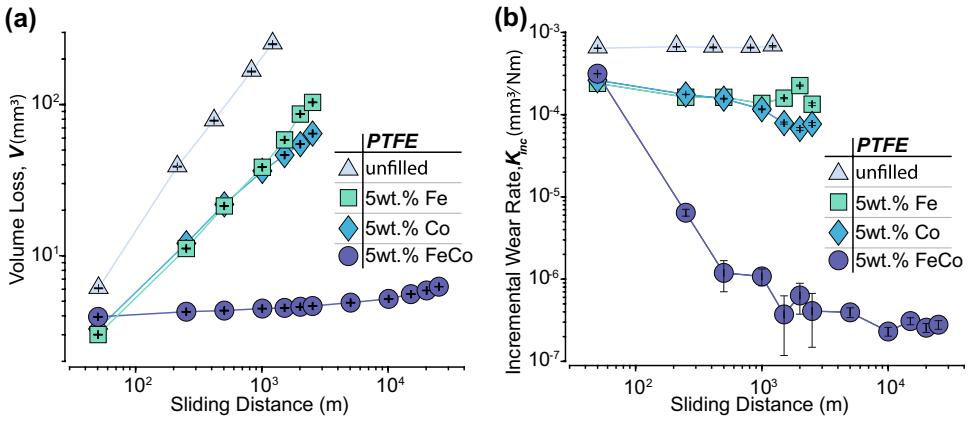

Fig. 4 **a** Volume loss V of unfilled PTFE, and PTFE filled with 5 wt% Fe, 5 wt% Co, and 5 wt% FeCo over the sliding distance. **b** Incremental wear rate of unfilled PTFE, 5 wt% Fe, 5 wt% Co, and 5 wt% FeCo

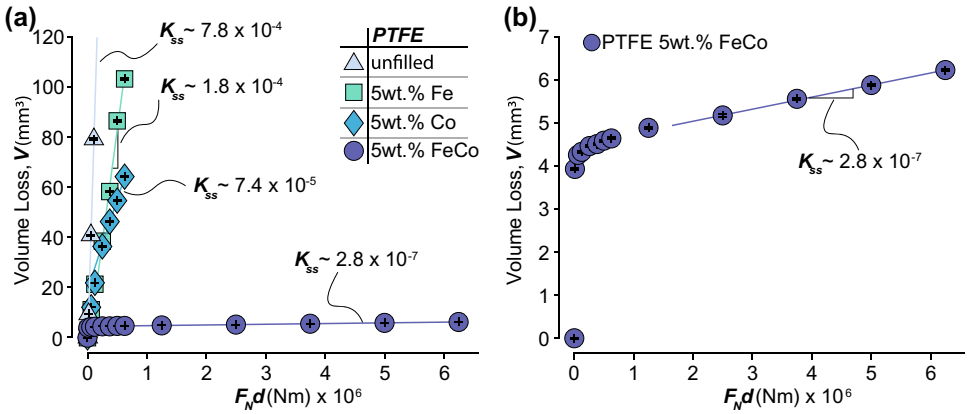

Fig. 5 **a** Volume loss V of unfilled PTFE, and PTFE filled with 5 wt% Fe, 5 wt% Co, and 5 wt% FeCo over the applied normal force times sliding distance, $F_N d$. Fe and Co composite samples were stopped at 2.5 km of sliding due to extremely high wear volume. **b** Volume loss of 5 wt% FeCo sample over the applied normal force times sliding distance. Plotted lines indicate regions in which steady-state wear was calculated (units in mm^3/Nm)

(Fig. 4b). After 1.5 km of sliding, PTFE–FeCo reached incremental wear rates on the order of 10^{-7} mm^3/Nm which were sustained for the rest of the experiment, achieving a steady-state wear rate of 2.8×10^{-7} mm^3/Nm. The steady-state wear behavior after 15 km of sliding can be observed in Fig. 4a, which shows a linear relationship with volume loss resulting in a constant incremental wear rate (Fig. 4b).

The run-in behavior of the PTFE–FeCo sample can be more closely inspected by plotting the volume loss over $F_N d$ (Fig. 5a and b). The total volume loss of the PTFE–Fe and PTFE–Co in the first 50 k sliding cycles (2.5 km) was 10–100× higher than that of the PTFE–FeCo sample. The steady-state wear rates of each sample are denoted by the lines plotted in Fig. 5a. Due to large differences in total volume loss between the PTFE–FeCo sample and the PTFE–Fe and PTFE–Co samples, we plot the volume loss as a function of $F_N d$ for the PTFE–FeCo sample in Fig. 5b to highlight the ultralow steady-state wear rate of PTFE–FeCo (2.8×10^{-7} mm^3/Nm).

A relationship between sliding distance and friction coefficient is observed when plotting the friction coefficient over the sliding distance (Fig. 6). The average friction coefficient was determined for logarithmically increasing sliding distances (1 m, 2 m, 5 m, 10 m, 20 m, 50 m, 100 m, etc.). A transition from a low friction coefficient ($\mu \sim 0.15$–0.16) to higher friction coefficient ($\mu \sim 0.21$–0.23) for the PTFE–FeCo sample is observed around 100 m of sliding and is indicated by a sharp increase in the coefficient of friction. The increase in the coefficient of friction appears to coincide with the incremental wear rate of PTFE–FeCo achieving an incremental

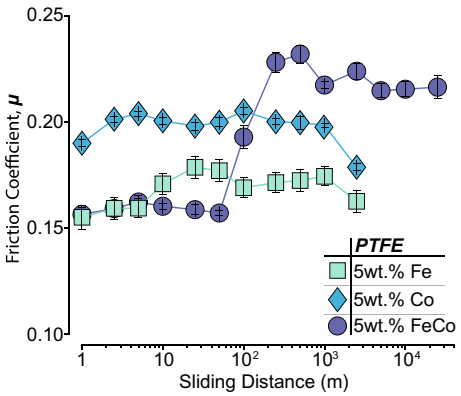

Fig. 6 Friction coefficient over the sliding distance of the experiment. Friction coefficient was determined at each point by averaging the friction at logarithmically increasing meters of sliding

wear rate on the order of 10^{-7} mm^3/Nm. The friction coefficients of the PTFE–Fe ($\mu \sim 0.17$) and PTFE–Co ($\mu \sim 0.20$) samples are lower than the final friction coefficients of the PTFE–FeCo sample, and only experience minor fluctuations throughout testing.

Optical images (Fig. 7a–c) and profilometry scans (Fig. 7d) of the transfer films formed by the Fe, Co, and FeCo-filled PTFE samples show distinct differences in color, thickness, and uniformity. The PTFE–Fe transfer film is thick, uniform, and rusty in color. The PTFE–Co transfer film is patchy, and the pin has caused deep scratching into the transfer film and metal substrate. The transfer film of the PTFE–FeCo sample is a combination of the constituent element transfer films—rusty in color like the PTFE–Fe transfer film and less uniform like the Co transfer film. The PTFE–FeCo transfer film also shows deposition of material at the reversals, which does not appear in the other transfer films.

4.3 IR Spectra

ATIR spectra of the polymer wear surface of the Fe, Co, and FeCo filled PTFE polymer pins were collected and normalized to the 1149 cm^{-1} peak, the symmetric stretch of CF_2 which is a characteristic peak of PTFE (Fig. 8a). All three samples showed similar -CF_2- peaks at 1204 cm^{-1} and 1149 cm^{-1}. Peaks at 1360 and 1317 cm^{-1} indicate shortened PTFE chains and are only present in the Fe and FeCo samples [20, 45, 46]. Iron oxide is present in both the Fe and FeCo samples, indicated by the 820 cm^{-1} peak. The characteristic cobalt oxide peak at 661 cm^{-1} is only observed in the Co sample. The peaks at 630 and 640 cm^{-1} can be attributed to CF_2 wagging and chain stretching of PTFE, respectively [47]. While this region looks identical in the Fe and FeCo samples, the Co sample only shares the 640 cm^{-1} peak. Peaks at 1660 cm^{-1} and 1430 cm^{-1} indicate the presence of perfluorinated carboxylates, which are referred to as

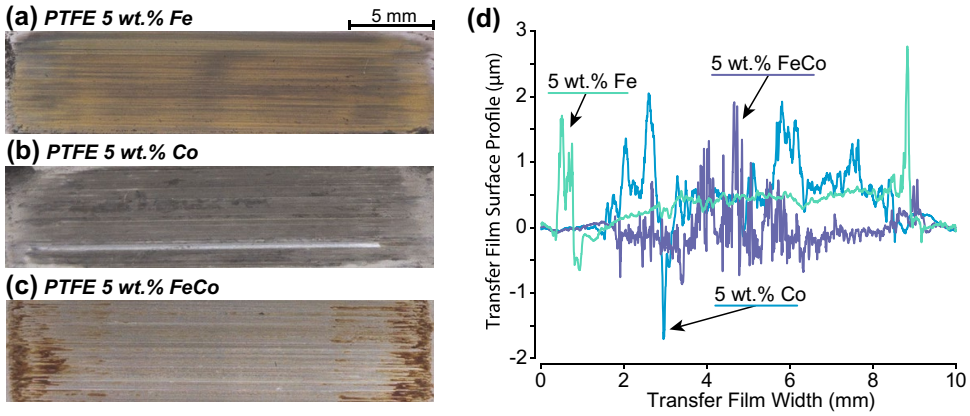

Fig. 7 Transfer films deposited on 304 SS counter sample for **a** PTFE 5 wt% Fe, **b** PTFE 5 wt% Co, and **c** PTFE 5 wt% FeCo. **d** Profilometry of transfer films on counter sample

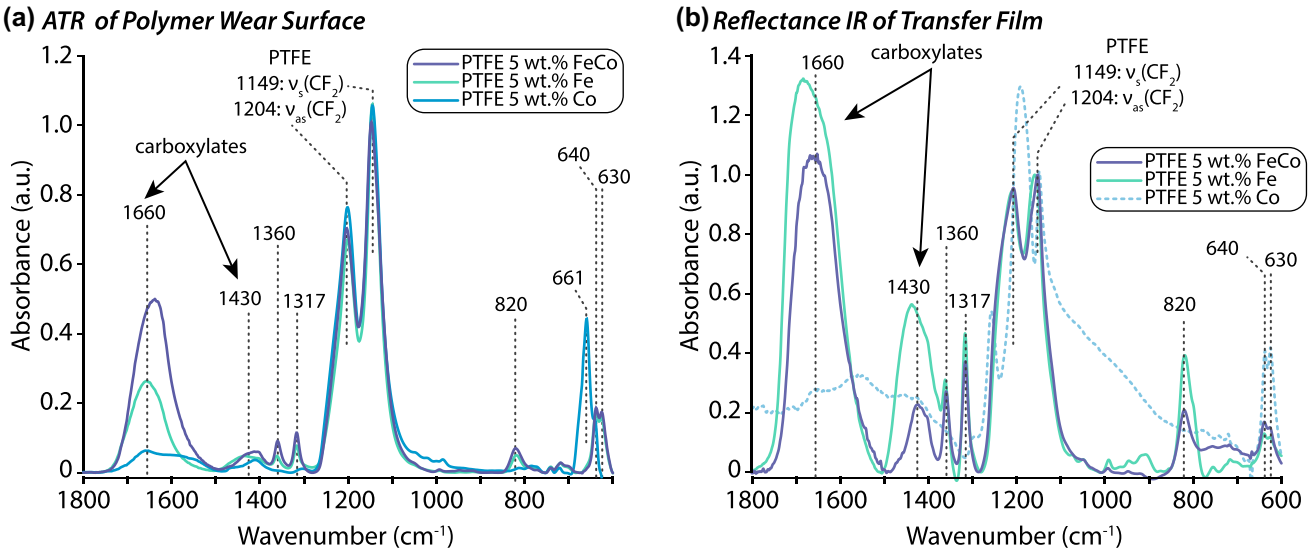

Fig. 8 **a** ATIR spectra of the worn polymer surface of the Fe, Co, and FeCo filled PTFE composites. **b** Reflectance IR spectra of the polymer transfer films on the surface of the stainless steel counter sample

tribochemical species (new chemical species formed during sliding) [17, 19, 24, 25, 48–50]. The FeCo polymer wear surface has the highest amount of carboxylates, the Fe polymer wear surface has slightly less, and the Co film has little carboxylates present in the polymer wear surface.

The chemical composition of the transfer films deposited on the counter sample during sliding was measured using reflectance IR at the conclusion of testing. The spectra were normalized to the 1149 cm^{-1} CF_2 peak (Fig. 8b). Similar CF_2 peaks at 1149 cm^{-1} and 1204 cm^{-1} and shortened PTFE chains at 1360 and 1317 cm^{-1} were observed in both the Fe and FeCo transfer films. The Fe and FeCo transfer films also have high levels of carboxylates present, shown by the peaks at 1660 cm^{-1} and 1430 cm^{-1}. The Fe transfer film had higher levels of carboxylates and iron oxides (820 cm^{-1}) present in the transfer films when compared to the FeCo transfer film. The spectra signal for the Co transfer film was very weak in comparison to the Fe and FeCo signals, most likely due to abrasion of the transfer film during sliding. This signal weakness made the spectra difficult to normalize and perform baseline subtraction, leading to some error in the measurement. It is worth noting that the Co transfer film had peaks in the CF_2 peak locations as well as a peak near the 1250 cm^{-1} region. This peak is not frequently observed experimentally, but is typically associated with very thin transfer films with aligned PTFE chains and can be found in PTFE transfer films after a single sliding cycle [19, 45, 51]. This could point to a very thin film of PTFE–Co that is suffering from abrasion, removal, and retransfer during sliding.

5 Discussion

PTFE filled with 5 wt% FeCo microparticles exhibited a steady-state wear rate of 2.8×10^{-7} mm^3/Nm, ~ 100× lower than PTFE filled with 5 wt% Co (7.4×10^{-5} mm^3/Nm) and ~ 1000× lower than PTFE filled with 5 wt% Fe (1.8×10^{-4} mm^3/Nm). The ultralow wear rate of PTFE–FeCo coincides with a well-developed transfer film and robust polymer wear surface, including the formation of tribochemical species. The evolution of the sliding interface due to tribochemical changes are observed by the increase in the coefficient of friction ($\mu \sim 0.22$) at 100 m of sliding (Fig. 5) and the subsequent decrease in volume loss and the incremental wear rate (Fig. 3a and b). This is similar to the transition in the coefficient of friction and wear rate in ultralow wear PTFE–alumina, which has previously been attributed to the development of transfer films and resulting increases in carboxylate accumulation and attractive forces at the interface [52]. The PTFE–Fe composite shows a minor increase in the coefficient of friction at 10 m of sliding (Fig. 5) yet does not experience a change in wear rate which is high (~ 10^{-4} mm^3/Nm) throughout the duration of the test.

IR spectroscopy of the polymer wear surfaces shows (Fig. 7) that the PTFE–FeCo sample accumulated the most carboxylates, indicated by the shoulders at 1660 cm^{-1} and 1430 cm^{-1}, and experienced the most PTFE chain shortening (peaks at 1360 and 1317 cm^{-1}). Shortening of PTFE chains has been observed in low-wear PTFE composites and is often paired with the formation of tribochemical species due to the reactivity of the R_F–$CF_2^{\cdot}$ radicals on the chain ends [7, 13, 19, 20, 24, 25, 46]. Accumulation of carboxylates provides anchor sites to metallic substrates creating well-adhered transfer films and polymer wear surfaces [13, 15, 19, 25, 26]. Interestingly, tribochemical infrared peaks are observed in both the FeCo and Fe samples, yet the tribological behavior is vastly different. The transfer films of the Fe and FeCo samples contained high amounts of carboxylates and iron oxide, with the Fe transfer film having higher levels when compared to the FeCo transfer films. The presence of carboxylates and PTFE chain scission in the Fe sample polymer wear surface and transfer film are indicative of a low-wear sample yet the PTFE–Fe has a wear rate (1.8×10^{-4} mm^3/Nm) on the order of virgin PTFE (~ 4–7 × 10^{-4} mm^3/Nm) [8, 10, 17]. The accumulation of carboxylates in a polymer wear surface of a PTFE composite with a high wear rate can be rationalized by considering competition between shear-induced carboxylate formation and wear events which remove interfacial species [53]. A possible explanation for the observed carboxylate accumulation in high wear PTFE–Fe running and transfer films is due to the reactive nature of iron causing further degradation of PTFE polymer chains at the sliding interface in conjunction with shear-induced degradation and chain scission [54].

A second explanation for the PTFE–Fe behavior stems from relationships between wear and surface energy [55]. Surface energy gradients between the polymer pin and the transfer film resulting from iron oxide and carboxylates in the transfer film drive material transfer from the polymer pin (*i.e.*, low to high surface energy) [55]. Though gradients in the surface energy can be beneficial for forming stable transfer films, large gradients can cause excessive wear. The high levels of carboxylates found in the transfer films of the PTFE–Fe sample indicate that there is significant degradation of PTFE chains and subsequent increases in the films surface energy as a result. It is possible that the PTFE–Fe sliding interface has an extremely high surface energy gradient that can result in high material transfer and wear of the pin. In the case of the PTFE–Co sample, the wear rate was ~ 2× lower than the PTFE–Fe sample (7.4×10^{-5} mm^3/Nm) yet the PTFE–Co polymer wear surface had the lowest amount of carboxylates present and had relatively small 1360 and 1317 cm^{-1} PTFE chain shortening peaks. The signal of the IR spectra in the transfer film was exceptionally low, with no observable carboxylates indicating that there was very little material transferred and retained on

the counter sample. The lack of tribochemical species and degraded PTFE chains could explain the poor wear rate which is only slightly better than virgin PTFE.

Microparticle fillers for PTFE composites must meet two criteria to achieve ultralow wear rates: (1) particles break up during sliding and accumulate at the sliding interface promoting the formation of carboxylates and (2) sub-surface particles need to arrest crack formation and prevent large-scale delamination events. PTFE filled with iron or cobalt microparticles appear to lack one of the two criteria required for ultralow wear, while PTFE–FeCo meets both. Interestingly, the particle morphology and size analysis of the Fe, Co, and FeCo particles do not correspond to the working mechanistic hypothesis for other ultralow wear materials like PTFE–alumina. In the PTFE–alumina wear system, the lowest wear particles are microscale particles with nanoscale primary particles or features, and are porous enough to break down during sliding [15]. Microscale, dense particles used as filler materials in PTFE tend to abrade the countersurface and disrupt transfer film formation [15, 16, 56]. Nanoscale particles lack the ability to reinforce the bulk polymer, and do not result in ultralow wear [15]. In the case of the Fe, Co, and FeCo powders, the particle size and apparent agglomerate morphology of the Fe and Co particles (Fig. 2a, b, f) would indicate that they could significantly reduce the wear rate of PTFE through reinforcement of the bulk polymer while also breaking down and accumulating at the sliding interface to reinforce tribofilms. By the same logic, the large, dense, micron-scale FeCo particles (Fig. 2c, f) would be expected to marginally improve the wear rate of PTFE but ultimately abrade the tribofilms and countersurface. However, the exact opposite wear behavior is observed when testing these filler particles.

The unexpected wear behavior of the Fe, Co, and FeCo microparticles indicates that particle size and morphology are not always the dominating factor in promoting ultralow wear. Particle friability and chemical interactions with reactive elements appear to dominate. While Fe promotes the formation of carboxylates and PTFE chain shortening, the particles cannot prevent sub-surface cracking and delamination, driving PTFE–Fe to be high wear. It seems that Fe microparticles can react with PTFE, causing excessive degradation at the sliding interface. Cobalt microparticles improved the wear rates of PTFE by reinforcing the bulk polymer and arresting sub-surface cracking and delamination events. Hard microscale particles have been shown to incrementally improve the wear rate of PTFE [15, 57]. Limited improvements in wear rates are a result of hard particles not breaking into smaller particles that accumulate at the surface during sliding but instead scratching the countersurface (Fig. 6b) and disrupting the formation of tribofilms [58]. While some alumina fillers are friable due to their porous, agglomerate nature, the agglomerate Co particles utilized in this study do not appear to be friable enough to promote ultralow wear [58]. Significant abrasion of the counter sample and transfer film could indicate that the Co particles are hard agglomerates that have difficulty breaking up during sliding. Additionally, even if the Co agglomerates are able to break up during sliding, the primary particles in the Co powder are ~ 1 μm in size, and at the smallest ~ 700 nm (Fig. 2a, d–f). Compared to the primary particles and nanoscale features observed in alumina fillers that promote ultralow wear (~ 40–80 nm) [15], the Co primary particles are 10–20× larger, and are still capable of abrading the counter sample and tribofilms.

We attribute the superior wear performance of the PTFE–FeCo sample to the same low-wear promoting mechanisms present in low filler wt% composites like PTFE–alumina, but with vastly different particle morphology and mechanical properties. Microscale FeCo particles reinforce the PTFE matrix and prevent sub-surface cracking and delamination. The inherent brittleness of FeCo alloys is a benefit for PTFE composites as it allows for the FeCo particles to break down into smaller particle sizes and accumulate during sliding, despite the dense, microscale state of the particles. Binary Fe–50Co that is utilized in this study as a metallic particle filler is characterized by low yield strength (200–300 MPa) and low strain-to-failure (0–6%) in tension, depending on the alloy processing thermal history [39, 59]. Specifically, the mechanical properties are significantly influenced by a characteristic phase transformation at ~ 730 °C in which a chemically disordered bcc lattice transitions to a chemically ordered B2 structure, impeding dislocation accommodation mechanisms during plastic deformation [38, 39]. The high temperature of the disorder–order transition leads to high-atomic mobility, making it difficult to avoid the ordered phase through conventional processing and can only be suppressed through rapid quenching from the high-temperature bcc phase region at rates in excess of 1000 °C/s [60]. In this study, FeCo was utilized as a gas atomized powder for a filler material and likely possesses some extent of the high-temperature disordered bcc phase due to rapid solidification associated with the powder processing. Note that cooling and solidification rates in gas atomization are unknown for the particular FeCo powder evaluated in this study, but previous literature has suggested cooling rates between 10^2 and 10^8 °C/s for gas atomization powder processing, which is sufficiently rapid to promote at least partial, if not full, chemical disorder in FeCo [60, 61]. Nonetheless, the powder filler itself is anticipated to have very limited ductility. In this study, therefore, the intrinsically brittle nature of the FeCo alloy is likely enabling the particles to break down as a result of sliding, subsequently accumulating in and reinforcing developing tribofilms. Without the brittle nature of the FeCo alloy, these filler particles would be expected to only promote marginal improvements

in the wear of PTFE while also abrading the countersurface and tribofilms, inhibiting ultralow wear behavior.

6 Conclusions

Iron, cobalt, and iron–cobalt microparticles are investigated as potential filler candidates for PTFE composites. Ultralow wear, low friction, magnetic polymer composites are created by filling PTFE with equiatomic, pre-alloyed FeCo microparticles. Particle size analysis and morphology indicate the Fe and Co microparticles are strongly fused agglomerates (10–20 μm) made of smaller primary features, while the FeCo microparticles are large (39 μm), spherical, dense particles. PTFE filled with 5 wt% FeCo achieves a steady-state wear rate of 2.8×10^{-7} mm^3/Nm and friction coefficient of 0.21. However, by comparison, PTFE filled with 5 wt% of Fe or Co microparticles exhibits wear rates only slightly lower than unfilled PTFE. PTFE–Co ($K \sim 7.4 \times 10^{-5}$ mm^3/Nm) has a ~ 10× improvement in wear when compared to unfilled PTFE, but improvements are limited by Co particles scratching the countersurface, preventing the development of robust transfer films. In contrast, PTFE–Fe ($K \sim 1.8 \times 10^{-4}$ mm^3/Nm) has a uniform and thick transfer film and relatively high levels of carboxylate accumulation but exhibits a wear rate on the order of unfilled PTFE. While Fe and Co microparticle fillers marginally improve the wear rate of PTFE, the filler particles appear to be too reactive and lack the necessary particle friability/nanoscale feature size, respectively. We attribute the ultralow wear behavior of PTFE–FeCo to the brittle nature of FeCo, which enables the microscale, metallic, and fully dense filler particles to break down during sliding while also reinforcing the bulk polymer by arresting sub-surface cracking and delamination.

Acknowledgements The authors would like to acknowledge Particle Technology Labs for performing the laser diffraction particle size measurements and analysis. We would like to thank Catherine Fidd for acquiring particle SEM images used in this study.

Funding This material is based upon work supported by the National Science Foundation CMMI MEP #2027029 (Krick CAREER), National Science Foundation CMMI MEP #1463141 (Krick GOALI), and National Science Foundation Graduate Research Fellowship Program under grant #1449440 (Van Meter), #1452783 (Campbell), and #1842163 (Babuska). Support from the Sandia National Laboratories Laboratory Directed Research and Development (LDRD) program is acknowledged. Sandia National Laboratories is a multimission laboratory managed and operated by National Technology and Engineering Solutions of Sandia LLC, a wholly owned subsidiary of Honeywell International Inc. for the U.S. Department of Energy's National Nuclear Security Administration under contract DE-NA0003525. This paper describes objective technical results and analysis. Any subjective views or opinions that might be expressed in the paper do not necessarily represent the views of the U.S. Department of Energy or the United States Government.

Data Availability The data that support the findings of this manuscript are available from the corresponding author upon reasonable request.

Declarations

Conflict of interest The authors have no competing interests to disclose.

References

1. Renfrew, M.M., Lewis, E.E.: Polytetrafluoroethylene Heat resistant, chemically inert plastic. Ind. Eng. Chem. **38**(9), 870–877 (1946). https://doi.org/10.1021/IE50441A009
2. Bunn, C.W., Cobbold, A.J., Palmer, R.P.: The fine structure of polytetrafluoroethylene. J. Polym. Sci. **28**(117), 365–376 (1958). https://doi.org/10.1002/pol.1958.1202811712
3. Bunn, C.W., Howells, E.R.: Structures of molecules and crystals of fluoro-carbons. Nature **174**(4429), 549–551 (1954). https://doi.org/10.1038/174549a0
4. Shooter, K.V., Tabor, D.: The frictional properties of plastics. Proc. Phys. Soc. Sect. B **65**(9), 661 (1952). https://doi.org/10.1088/0370-1301/65/9/302
5. Puts, G.J., Crouse, P., Ameduri, B.M.: Polytetrafluoroethylene: synthesis and characterization of the original extreme polymer. Chem. Rev. (2019). https://doi.org/10.1021/ACS.CHEMREV.8B00458
6. Bahadur, S., Tabor, D.: The wear of filled polytetrafluoroethylene. Wear **98**(1), 1–13 (1984). https://doi.org/10.1016/0043-1648(84)90213-8
7. Biswas, S.K., Vijayan, K.: Friction and wear of PTFE—a review. Wear **158**(1–2), 193–211 (1992). https://doi.org/10.1016/0043-1648(92)90039-B
8. Makinson, K.R., Tabor, D.: Friction and transfer of polytetrafluoroethylene. Nature **201**(1), 464–466 (1964). https://doi.org/10.1038/201464a0
9. Tanaka, K., Uchiyama, Y., Toyooka, S.: The mechanism of wear of polytetrafluoroethylene. Wear **23**(2), 153–172 (1973). https://doi.org/10.1016/0043-1648(73)90081-1
10. Blanchet, T.A., Kennedy, F.E.: Sliding wear mechanism of polytetrafluoroethylene (PTFE) and PTFE composites. Wear **153**(1), 229–243 (1992). https://doi.org/10.1016/0043-1648(92)90271-9
11. Tanaka, K.: Effects of various fillers on the friction and wear of PTFE-based composites. Compos. Mater. Ser. **1**(C), 137–174 (1986). https://doi.org/10.1016/B978-0-444-42524-9.50009-0
12. Burris, D.L., Sawyer, W.G.: Improved wear resistance in alumina-PTFE nanocomposites with irregular shaped nanoparticles. Wear **260**, 915–918 (2006). https://doi.org/10.1016/j.wear.2005.06.009
13. Krick, B.A., Ewin, J.J., Blackman, G.S., Junk, C.P., Gregory Sawyer, W., Sawyer, W.G.: Environmental dependence of ultra-low wear behavior of polytetrafluoroethylene (PTFE) and alumina composites suggests tribochemical mechanisms. Tribiol. Int. **51**, 42–46 (2012). https://doi.org/10.1016/j.triboint.2012.02.015
14. Krick, B.A., Ewin, J.J., McCumiskey, E.J.: Tribofilm formation and run-in behavior in ultra-low-wearing polytetrafluoroethylene (PTFE) and alumina nanocomposites. Tribol. Trans. **57**(6), 1058–1065 (2014). https://doi.org/10.1080/10402004.2014.933934
15. Krick, B.A., et al.: Ultralow wear fluoropolymer composites: nanoscale functionality from microscale fillers. Tribol. Int. **95**, 245–255 (2016). https://doi.org/10.1016/J.TRIBOINT.2015.10.002
16. Burris, D.L., Boesl, B., Bourne, G.R., Sawyer, W.G.: Polymeric nanocomposites for tribological applications. Macromol. Mater.

Eng. **292**(4), 387–402 (2007). https://doi.org/10.1002/mame.200600416
17. Van Meter, K.E., Junk, C.P., Campbell, K.L., Babuska, T.F., Krick, B.A.: Ultralow wear self-mated PTFE composites. Macromolecules (2022). https://doi.org/10.1021/ACS.MACROMOL.1C02581
18. Pitenis, A.A., Ewin, J.J., Harris, K.L., Sawyer, W.G., Krick, B.A.: In vacuo tribological behavior of polytetrafluoroethylene (PTFE) and alumina nanocomposites: the importance of water for ultralow wear. Tribol. Lett. **53**(1), 189–197 (2013). https://doi.org/10.1007/S11249-013-0256-1
19. Harris, K.L., et al.: PTFE tribology and the role of mechanochemistry in the development of protective surface films. ACS Macromol. (2015). https://doi.org/10.1021/acs.macromol.5b00452
20. Khare, H.S., et al.: Interrelated effects of temperature and environment on wear and tribochemistry of an ultralow wear PTFE composite. J. Phys. Chem. C **119**(29), 16518–16527 (2015). https://doi.org/10.1021/ACS.JPCC.5B00947
21. Burris, D.L., Sawyer, W.G.: Tribological behavior of PEEK components with compositionally graded PEEK/PTFE surfaces. Wear **262**(1–2), 220–224 (2007). https://doi.org/10.1016/J.WEAR.2006.03.045
22. Burris, D.L., et al.: A route to wear resistant PTFE via trace loadings of functionalized nanofillers. Wear **267**, 653–660 (2009). https://doi.org/10.1016/j.wear.2008.12.116
23. Burris, D.L., Sawyer, W.G.: A low friction and ultra low wear rate PEEK/PTFE composite. Wear **261**(3–4), 410–418 (2006). https://doi.org/10.1016/j.wear.2005.12.016
24. Campbell, K.L., et al.: Ultralow Wear PTFE-based polymer composites—the role of water and tribochemistry. Macromolecules **52**(14), 5268–5277 (2019). https://doi.org/10.1021/acs.macromol.9b00316
25. Pitenis, A.A., et al.: Ultralow wear PTFE and alumina composites: it is all about tribochemistry. Tribol. Lett. (2015). https://doi.org/10.1007/s11249-014-0445-6
26. Alam, K.I., Baratz, A., Burris, D.: Leveraging trace nanofillers to engineer ultra-low wear polymer surfaces. Wear **482–483**, 203965 (2021). https://doi.org/10.1016/J.WEAR.2021.203965
27. Bhargava, S., Blanchet, T.A.: Unusually effective nanofiller a contradiction of microfiller-specific mechanisms of PTFE composite wear resistance? J. Tribol. (2016). https://doi.org/10.1115/1.4032818/377872
28. McElwain, S.E., Blanchet, T.A., Schadler, L.S., Sawyer, W.G.: Effect of particle size on the wear resistance of alumina-filled PTFE micro- and nanocomposites. Tribol. Trans. **51**(3), 247–253 (2008). https://doi.org/10.1080/10402000701730494
29. Ullah, S., Haque, F.M., Sidebottom, M.A.: Maintaining low friction coefficient and ultralow wear in metal-filled PTFE composites. Wear **498–499**, 204338 (2022). https://doi.org/10.1016/J.WEAR.2022.204338
30. Tabor, D.D.: Friction, lubrication, and wear. In: Rothbart, H., Brown, T. (eds.) Mechanical Design Handbook, 2nd edn. McGraw-Hill, New York (2006)
31. Totten, G.E., et al.: ASM Handbook, Vol. 18: Friction, Lubrication, and Wear Technology. ASM International, Materials Park (2017)
32. Aldousiri, B., Shalwan, A., Chin, C.W.: A review on tribological behaviour of polymeric composites and future reinforcements. Adv. Mater. Sci. Eng. (2013). https://doi.org/10.1155/2013/645923
33. Valente, C.A.G.S., Boutin, F.F., Rocha, L.P.C., do Vale, J.L., da Silva, C.H.: Effect of graphite and bronze fillers on PTFE tribological behavior: a commercial materials evaluation. Tribol. Trans. **63**(2), 356–370 (2020). https://doi.org/10.1080/10402004.2019.1695032
34. Trabelsi, M., Kharrat, M., Dammak, M.: On the friction and wear behaviors of PTFE based composites filled with MoS2 and/or bronze particles. Trans. Indian Inst. Met. **69**(5), 1119–1128 (2016). https://doi.org/10.1007/s12666-015-0666-x
35. Khan, M.J., Wani, M.F., Gupta, R.: Tribological properties of bronze filled PTFE under dry sliding conditions and aqueous environments (distilled water and sea water). Int. J. Surf. Sci. Eng. **12**(5–6), 348–364 (2018). https://doi.org/10.1504/IJSURFSE.2018.096742
36. Wang, Y., Yan, F.: A study on tribological behaviour of transfer films of PTFE/bronze composites. Wear **262**(7–8), 876–882 (2007). https://doi.org/10.1016/j.wear.2006.08.026
37. Unal, H., Kurtulus, E., Mimaroglu, A., Aydin, M.: Tribological performance of PTFE bronze filled composites under wide range of application conditions. J. Reinforced Plastics Compos. (2010). https://doi.org/10.1177/0731684409345617
38. Sundar, R.S., Deevi, S.C.: Soft magnetic FeCo alloys: alloy development, processing, and properties. Int. Mater. Rev. **50**(3), 157–192 (2005). https://doi.org/10.1179/174328005X14339
39. Sourmail, T.: Near equiatomic FeCo alloys: constitution, mechanical and magnetic properties. Prog. Mater. Sci. **7**, 816–880 (2005). https://doi.org/10.1016/j.pmatsci.2005.04.001
40. Kustas, A.B., et al.: Characterization of the Fe–Co–1.5V soft ferromagnetic alloy processed by Laser Engineered Net Shaping (LENS). Addit. Manuf. **21**(1), 41–52 (2018). https://doi.org/10.1016/J.ADDMA.2018.02.006
41. Kawahara, K.: Effect of additive elements on cold workability in FeCo alloys. J. Mater. Sci. **18**(6), 1709–1718 (1983). https://doi.org/10.1007/BF00542066
42. Schmitz, T.L., Action, J.E., Burris, D.L., Ziegert, J.C., Sawyer, W.G.: Wear-rate uncertainty analysis. J. Tribol. **126**(4), 802–808 (2004). https://doi.org/10.1115/1.1792675
43. Schmitz, T.L., Action, J.E., Ziegert, J.C., Sawyer, W.G.: The difficulty of measuring low friction: uncertainty analysis for friction coefficient measurements. Trans. ASME (2005). https://doi.org/10.1115/1.1843853
44. Burris, D.L., Sawyer, W.G.: Addressing practical challenges of low friction coefficient measurements. Tribol. Lett. **35**(1), 17–23 (2009). https://doi.org/10.1007/s11249-009-9438-2
45. Lauer, J.L., Bunting, B.G., Jones, W.R., Jr.: Investigation of frictional transfer films of PTFE by infrared emission spectroscopy and phase-locked ellipsometry. Tribol. Trans. **31**(2), 282–288 (1988). https://doi.org/10.1080/10402008808981824
46. Vanni, H., Rabolt, J.F.: Fourier transform infrared investigation of the effects of irradiation on the 19 and 30°C phase transitions in polytetrafluoroethylene. J. Polym. Sci. Polym. Phys. Ed. **18**(3), 587–596 (1980). https://doi.org/10.1002/POL.1980.180180317
47. Liang, C.Y., Krimm, S.: Infrared spectra of high polymers. III. Polytetrafluoroethylene and polychlorotrifluoroethylene. J. Chem. Phys. **25**(3), 563 (2004). https://doi.org/10.1063/1.1742964
48. Przedlacki, M., Kajdas, C.: Tribochemistry of fluorinated fluids hydroxyl groups on steel and aluminum surfaces. Tribol. Trans. **49**(2), 202–214 (2006). https://doi.org/10.1080/05698190500544676
49. Kajdas, C.K.: Importance of the triboemission process for tribochemical reaction. Tribol. Int. **38**(3), 337–353 (2005). https://doi.org/10.1016/J.TRIBOINT.2004.08.017
50. Haidar, D.R., Alam, K.I., Burris, D.L.: Tribological insensitivity of an ultralow-wear poly(etheretherketone)-polytetrafluoroethylene polymer blend to changes in environmental moisture. J. Phys. Chem. C **122**(10), 5518–5524 (2018). https://doi.org/10.1021/acs.jpcc.7b12487
51. Moynihan, R.E.: The molecular structure of perfluorocarbon polymers. Infrared studies on polytetrafluoroethylene1. J. Am. Chem.

Soc. **81**(5), 1045–1050 (2002). https://doi.org/10.1021/JA01514A009
52. Krick, B.A.: Exploring the Ultra-Low Wear Behavior of Polytetrafluoroethylene and Alumina Composites. University of Florida, Gainesville (2012)
53. Alam, K.I., Burris, D.L.: Ultralow wear poly(tetrafluoroethylene): a virtuous cycle of wear reduction and tribochemical accumulation. J. Phys. Chem. C **125**(35), 19417–19427 (2021). https://doi.org/10.1021/ACS.JPCC.1C03885
54. Onodera, T., Nakakawaji, T., Adachi, K., Kurihara, K., Kubo, M.: Tribochemical degradation of polytetrafluoroethylene catalyzed by copper and aluminum surfaces. J. Phys. Chem. C **120**(20), 10857–10865 (2016)
55. Ye, J., et al.: Interfacial gradient and its role in ultralow wear sliding. J. Phys. Chem. (2020). https://doi.org/10.1021/acs.jpcc.9b12036
56. Bahadur, S.: The development of transfer layers and their role in polymer tribology. Wear **245**(1–2), 92–99 (2000). https://doi.org/10.1016/S0043-1648(00)00469-5
57. Sawyer, W.G., Freudenberg, K.D., Bhimaraj, P., Schadler, L.S.: A study on the friction and wear behavior of PTFE filled with alumina nanoparticles. Wear **254**(5–6), 573–580 (2003). https://doi.org/10.1016/S0043-1648(03)00252-7
58. Sidebottom, M.A., Babuska, T.F., Ullah, S., Heckman, N., Boyce, B.L., Krick, B.A.: Nanomechanical filler functionality enables ultralow wear polytetrafluoroethylene composites. ACS Appl. Mater. Interfaces (2022). https://doi.org/10.1021/acsami.2c13644
59. George, E.P., Gubbi, A.N., Baker, I., Robertson, L.: Mechanical properties of soft magnetic FeCo alloys. Mater. Sci. Eng. **329–331**, 325–333 (2002)
60. Clegg, D.W., Buckley, R.A.: The disorder → order transformation in iron–cobalt-based alloys. Met. Sci. J. **7**(1), 48–54 (1973). https://doi.org/10.1179/030634573790445541
61. Mullis, A.M., Farrell, L., Cochrane, R.F., Adkins, N.J.: Estimation of cooling rates during close-coupled gas atomization using secondary dendrite arm spacing measurement. Metall. Mater. Trans. B Process Metall. Mater. Process. Sci. **44**(4), 992–999 (2013). https://doi.org/10.1007/s11663-013-9856-2